Available online at www.sciencedirect.com
ScienceDirect
Catalysis Today 127 (2007) 103–112
CATALYSIS TODAY
www.elsevier.com/locate/cattod

The gas–liquid contacting effect on the operation of small scale upflow hydrotreaters

G.D. Bellos, K.P. Gotsis, N.G. Papayannakos *

National Technical University of Athens, School of Chemical Engineering, Heroon Polytechniou 9, 157 80 Zografos, Greece

Available online 3 July 2007

Abstract

The effect of reactor geometry and bed dilution on the extent of gas oil hydrodesulfurization was tested by conducting hydrodesulfurization experiments in two laboratory reactors of different scale with non-diluted and diluted beds in ascending flow. The superficial gas and liquid velocities and the catalyst bed height were kept constant while the main difference between the two reactor scales was the reactor diameter. The diluted bed of the mini-reactor showed the best performance and its results were identical in upflow and downflow mode. The differences between the performance of the mini- and the bench-scale reactor operating in upflow mode have been investigated. Reactor performance simulation was attempted by a mathematical model that takes into account axial dispersion of the liquid phase and gas–liquid mass transfer. Bench-scale reactor operation was characterized by lower mass transfer rates than the corresponding mini-scale one. Combining model predictions and mock up operation it is concluded that the stronger mass transfer resistances calculated for the bench-scale reactor are associated with poorer gas distribution through the catalyst bed. Reduction of the bed diameter results in better gas–liquid contact by forcing the gas bubbles to distribute more effectively into the liquid phase.

Keywords: Dispersion; Hydrodesulfurization; Mass transfer; Multiphase reactors; Packed bed; Scale-up

1. Introduction

Downscaling is not only a means to obtain cheaper, faster and in a safer way experimental data but also a way to study process characteristics. A crucial and difficult in most cases to achieve task is the decoupling of reaction rates from the fluid dynamics and mass transfer effects. The latter effects are strictly connected with the laboratory reactors employed in experimentation while kinetics should not be affected by the reactor size and shape. Therefore, the estimation of the impact of these effects on reactor performance is indispensable in kinetic, catalyst and scale up/down studies.

Three phase hydrotreaters are widely used in petroleum industry and the importance of hydrotreatment in producing cleaner fuels and upgrading heavy feeds has lately adds to the interest in applications and research for improved efficiency. Experimental data is mostly obtained from small scale hydrotreaters and the controlling parameters of their performance should always be taken into account in modeling and interpretation of the results. Liquid phase non-ideal flow has been proved to be a very important hydrodynamic parameter in small scale laboratory hydrotreaters and its extent is widely estimated by using the axial dispersion model. Gas–liquid mass transfer may also affect reactor performance and its impact on overall reaction rates can be assessed using the film theory.

The bed dilution and the application of the concurrent upflow mode are the main ways that have been suggested in literature [1–5] in order to eliminate the non-ideal flow effects and enhance the particle wetting efficiency. Catalyst dilution with inert fines diminishes the liquid axial dispersion and improves wetting efficiency in downflow reactors too. Therefore, the conversions achieved by diluted beds operating in upflow mode are in many cases higher than the corresponding ones obtained by non-diluted beds in downflow mode. However, it is practically difficult to verify that all the multiphase effects and resistances affecting reaction rates are minimized or diminished due to the lack of adequate transfer and dispersion data as concerns small scale three phase reactors. But, the possible deviations in operation of different scale reactors should always be explained and the reasons of deviations quantitatively substantiated.

* Corresponding author. Tel.: +30 210 772 3239; fax: +30 210 772 3155.
E-mail address: npap@central.ntua.gr (N.G. Papayannakos).

0920-5861/$ – see front matter © 2007 Elsevier B.V. All rights reserved.
doi:10.1016/j.cattod.2007.05.004

Nomenclature

A	pre-exponential factor of activity $(l_L^n/h\ (mol\ i)^{n-1}\ g_{CAT})$
c_1–c_6	constants in Eqs. (21) and (22)
C	concentration (mol l^{-1})
D_{AX}	axial dispersion coefficient ($mm^2\ s^{-1}$)
D_{ij}	diffusivity ($mm^2\ s^{-1}$)
$D^L_{i,eff}$	effective diffusivity ($mm^2\ s^{-1}$)
D^0_{ij}	molecular diffusion ($mm^2\ s^{-1}$)
E	activation energy (kJ $mol^{-1}\ K^{-1}$)
H	Henry coefficient $((mol_i\ l^{-1})_G/(mol_i\ l^{-1})_L)$
H/C	hydrocarbons
k	specific reaction constant $(l_L^n/h\ (mol\ i)^{n-1}\ g_{CAT})$
K_{H_2S}	inhibition factor of H_2S $(mol\ H_2S\ l_L^{-1})$
$k_{L,i}$	liquid side mass transfer coefficient $(m_L^3\ m_{interface}^{-2}\ s^{-1})$
K_{LG}	gas–liquid mass transfer coefficient $(m_L^3\ m_{interface}^{-2}\ s^{-1})$
ℓ	local position along the reactor length (m)
L	bed height (m)
n	reaction order
R	reaction rate $(mol\ g_{CAT}^{-1}\ h^{-1})$
R_G	ideal gas constant = 8.314 (J mol^{-1})
S	stoichiometric coefficient
T	absolute temperature (K)
ΔT	thermal increment (K)
u	velocity ($mm\ s^{-1}$)
WHSV	space velocity $(kg_{oil}/kg_{cat}\ h)$
x	molecular fraction in the liquid phase
y	molecular fraction in the gas phase

Greek letters

α_V	interfacial area $(m^2_{interfacial}\ m^{-3}_{reactor})$
β	hold up $(m^3_{liquid\ or\ gas}\ m^{-3}_{void})$
δ	film thickness
ε	porosity $(m^3_{void}\ m^{-3}_{bed})$
η	apparent catalytic activity
ρ	density (g ml^{-1})

Index

AX	axial
B	typical HDS conditions
BED	bed
CAT	catalyst
effect	effective
G	gas
HDS	hydrodesulfurization reaction
HYD	saturation reaction
i	compound index number
L	liquid
S	superficial

Various sizes of laboratory, pilot and large scale hydrotreaters have been referred in literature. In Table 1, the definition of the reactor scale proposed by Gierman [6] is presented. The same terminology has been used by other authors defining as microreactors [3,5,7,8] the reactors with bed volume from 2 to 10 ml. The diameter and length of these reactors are around 10 and 130 mm, respectively, which are beyond the micrometer order of magnitude. In contrary, the flow rates and the superficial velocities for LHSV = 1 h^{-1} for a bed volume of 10 ml are 2.8 μl s^{-1} and 35 μm s^{-1} which are in the micrometer order of magnitude and consequently the attribution of this definition is reasonable. In more recent works [9,10] the term microreactor is attributed to devices with parallel channels having diameters of some micrometers. In this case the term microreactor is used on account of the channel diameter and the methods of catalyst deposition on the walls. The latter type of reactor is applied yet for one or two phase reactions conducted at mild conditions. Therefore, the term ''mini-reactor'' is proposed to be used for the reactors with 2–10 ml catalytic bed volume in order to avoid the eventual confusion with the novel type micro-channels reactors.

Table 1
Reactors scales definition by Gierman [6]

Reactor category	Catalytic bed volume (ml)
Nanoflow	0.5
Microflow	5
Bench scale	50
Small pilot plant	500
Large pilot plant	5000

The scope of this paper is to investigate the effect of scaling down of three phase upflow hydrotreaters. To this end, the apparent catalytic activity of a mini- (5.5 g of catalyst) and a bench-scale reactor (50 g of catalyst) is compared by examining diluted and non-diluted beds. The differences in performance of the upflow reactors, for which liquid dispersion data are available, have been studied and the mass transfer resistances in both reactors have been estimated and discussed.

2. Experimental section

All the hydrodesulfurization experiments were carried out with a straight run atmospheric gas oil (1.45 wt.% S) and a Ni–Mo/γ-Al_2O_3 commercial catalyst in cylindrical form with a mean diameter of 1.15 mm and particle density 1.3 g cm^{-3}. In the case of diluted beds, Silicon carbide fines with a mean diameter of 250 μm were used. A mini-scale reactor of 8 mm internal diameter was used to study the behavior of a non-diluted and a diluted bed.

The bed height of the non-diluted and the diluted bed was 14 and 16.9 cm, respectively, while both beds were loaded with 5.5 g of catalyst extrudates. The expansion of the diluted bed is due to the excess of the diluent fines used for the catalyst bed dilution. The same feed and catalyst system was used in a previous work [11]. The operating temperature of the mini-reactor was measured at several points on its external wall and the maximum difference was 0.5 °C. Thermal tests with an internal traveling thermocouple have verified that the temperature difference between the catalyst bed and the external wall was less than 1 °C for all the experimental conditions of this work and the forced convection isothermal heater used.

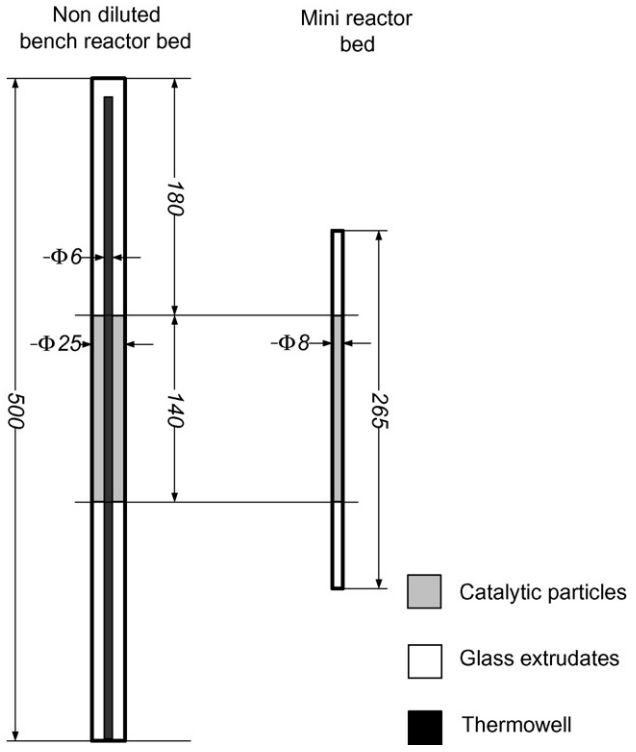

Fig. 1. Configuration of catalytic beds in bench and mini-scale reactors.

Two catalytic beds were examined in a bench-scale reactor of 25 mm internal diameter equipped with a 6 mm external diameter thermowell. The first bed was non-diluted and the second one diluted by the same procedure as the mini-scale reactor. The length of the non-diluted bed was 14 cm and of the diluted one 17.2 cm while their catalytic mass were 52.7 and 50.5 g, respectively. The silicon carbide to catalyst ratio was equal to 1.2 g_{SiC}/g_{CAT} in both reactors. Going down from the bench to the mini-reactor size, the bed height was kept constant and so the superficial velocities were also kept constant at the same space velocities. A graphic representation of the beds loaded in the bench and the mini-scale reactors is depicted in Fig. 1.

The experiments in both reactors were conducted at 54 bar in a temperature range of 30 K, by varying WHSV from 1 to 2 h^{-1} and the gas to oil ratio from 500 to 1000 Nl/kg. The experimental conditions, the superficial gas and liquid velocities for each experimental point for both reactors, Reynolds and Schmidt numbers for both phases are given in Table 2. It is noted that dimensionless numbers are calculated at reactor inlet conditions and get identical values for both reactor scales. Gas and liquid were pre-mixed before the reactor entrance and they entered the reactor through a tube opening of 3 mm. This is the simplest and most commonly used feeding system. Therefore, the distribution of the gas phase was achieved by the same way in both reactor types through the beds supporting layers. Quartz wool layers of 5 mm thickness were placed at the top and bottom of each bed of supporting inert glass extrudates to enhance gas–liquid distribution.

3. Mathematical model

For the simulation of the gas oil HDS reactor it is essential to evaluate the gas oil evaporation as well as the hydrogen and hydrogen sulfide solubility in the oil fraction at reaction conditions. For this reason the petroleum fraction can be simulated with a number of pseudo-components that represent the real molecules of the hydrocarbon mixture [11]. In this work, four components with identical physicochemical characteristics simulate the behavior of the reactants and products in gas oil. The first component ($i = 1$) represents the non-saturated hydrocarbon molecules that can be hydrogenated during hydrotreatment, the second one ($i = 2$) the sulfur bearing organic compounds, while the third ($i = 3$) stands for the organic desulfurized products and the fourth pseudo-compound ($i = 4$) for the saturated hydrocarbons produced by the hydrogenation reactions.

The developed model takes into account two kinetic equations. One equation describes the hydrodesulfurization reaction rates (Eq. (1)) of the molecules bearing sulfur atoms. A second kinetic equation gives the hydrogen consumption (Eq. (2)) due to hydrogenation of the non-saturated compounds. Both kinetic equations are of Langmuir–Hinshelwood type with a H_2S inhibition factor. Liquid solid mass transfer has been neglected allowing the assumption that the liquid in contact with catalyst particles has the same composition as the bulk liquid phase:

$$R_{\mathrm{HDS},i} = k_{\mathrm{HDS}} \frac{C_{\mathrm{L},i}^{n_{\mathrm{HDS}}} C_{\mathrm{L,H_2}}}{1 + K_{\mathrm{H_2S,HDS}} C_{\mathrm{L,H_2S}}} = A_{\mathrm{HDS}}\, \mathrm{e}^{-E_{\mathrm{HDS}}/(R_{\mathrm{G}} \cdot T)} \frac{C_{\mathrm{L},i}^{n_{\mathrm{HDS}}} C_{\mathrm{L,H_2}}}{1 + K_{\mathrm{H_2S,HDS}} C_{\mathrm{L,H_2S}}} \quad (1)$$

$$R_{\mathrm{HYD},i} = k_{\mathrm{HYD}} \frac{C_{\mathrm{L},i}^{n_{\mathrm{HYD}}} C_{\mathrm{L,H_2}}}{1 + K_{\mathrm{H_2S,HYD}} C_{\mathrm{L,H_2S}}} = A_{\mathrm{HYD}}\, \mathrm{e}^{-E_{\mathrm{HYD}}/(R_{\mathrm{G}} \cdot T)} \frac{C_{\mathrm{L},i}^{n_{\mathrm{HYD}}} C_{\mathrm{L,H_2}}}{1 + K_{\mathrm{H_2S,HYD}} C_{\mathrm{L,H_2S}}} \quad (2)$$

Table 2
Gas and liquid superficial velocities for all the experimental conditions for both reactors

T (K)	WHSV (h^{-1})	G/L (Nl/l)	u_{LS} (mm s^{-1})	u_{GS} (mm s^{-1})	Evaporation (wt.%)	Liquid phase			Gas phase		
						Re_L	Schmidt number		Re_G	Schmidt number	
							H/C	H_2		H/C	H_2
593	1	1000	0.029	1.38	36.4	0.13	33.1	13.3	2.05	33.1	13.3
613	1	1000	0.023	1.44	49.9	0.1	24.5	11.3	2.66	24.5	11.3
623	2	500	0.061	1.43	34.3	0.31	21.3	9.6	3.28	21.3	9.6

The mathematical model consists of the mass balances of the liquid and gas phase and of the total continuity equations of both phases. In the mass balances of the liquid phase the reaction, the axial dispersion and the gas–liquid mass transfer terms are taken into account. In the gas phase mass balances the gas–liquid mass transfer term was used but no reaction term has been inserted as it is assumed that the catalyst is completely wetted by reason of the upflow mode of operation and only the liquid phase is in contact with the catalyst active sites. Also, the gas phase mass balances are based on the plug flow regime. The general simulation model accounting for gas–liquid mass transfer resistances and liquid phase non-ideal flow is given below:

- Liquid phase mass balance for the component representing the non saturated compounds ($i = 1$):

$$\frac{\mathrm{d}(u_\mathrm{L}C_\mathrm{L}x_i)}{\mathrm{d}\ell} = \frac{\mathrm{d}}{\mathrm{d}\ell}\left(D_\mathrm{AX}C_\mathrm{L}\frac{\mathrm{d}x_i}{\mathrm{d}\ell}\right) + \frac{K_{\mathrm{LG},i}\alpha_\mathrm{V}}{\varepsilon\cdot\beta_\mathrm{L}}\left(\frac{C_\mathrm{G}y_i}{H_i} - C_\mathrm{L}x_i\right) - \frac{\rho_\mathrm{BED}}{\varepsilon\cdot\beta_\mathrm{L}}\left(A_\mathrm{HYD}\,\mathrm{e}^{-(E_\mathrm{HYD}/RT)}C_\mathrm{L}^{1+n_\mathrm{HYD}}\right)\frac{x_i^{n_\mathrm{HYD}}x_{\mathrm{H_2}}}{1+K_{\mathrm{H_2S,HYD}}C_\mathrm{L}x_{\mathrm{H_2S}}} \tag{3}$$

- Liquid phase mass balance for the component representing the sulfur bearing organic compounds ($i = 2$):

$$\frac{\mathrm{d}(u_\mathrm{L}C_\mathrm{L}x_i)}{\mathrm{d}\ell} = \frac{\mathrm{d}}{\mathrm{d}\ell}\left(D_\mathrm{AX}C_\mathrm{L}\frac{\mathrm{d}x_i}{\mathrm{d}\ell}\right) + \frac{K_{\mathrm{LG},i}\alpha_\mathrm{V}}{\varepsilon\cdot\beta_\mathrm{L}}\left(\frac{C_\mathrm{G}y_i}{H_i} - C_\mathrm{L}x_i\right) - \frac{\rho_\mathrm{BED}}{\varepsilon\cdot\beta_\mathrm{L}}\left(A_\mathrm{HDS}\,\mathrm{e}^{-E_\mathrm{HDS}/RT}C_\mathrm{L}^{1+n_\mathrm{HDS}}\right)\frac{x_i^{n_\mathrm{HDS}}x_{\mathrm{H_2}}}{1+K_{\mathrm{H_2S,HDS}}C_\mathrm{L}x_{\mathrm{H_2S}}} \tag{4}$$

- Liquid phase mass balance for the component representing the organic hydrodesulphurized products ($i = 3$):

$$\frac{\mathrm{d}(u_\mathrm{L}C_\mathrm{L}x_i)}{\mathrm{d}\ell} = \frac{\mathrm{d}}{\mathrm{d}\ell}\left(D_\mathrm{AX}C_\mathrm{L}\frac{\mathrm{d}x_i}{\mathrm{d}\ell}\right) + \frac{K_{\mathrm{LG},i}\alpha_\mathrm{V}}{\varepsilon\cdot\beta_\mathrm{L}}\left(\frac{C_\mathrm{G}y_i}{H_i} - C_\mathrm{L}x_i\right) + \frac{\rho_\mathrm{BED}}{\varepsilon\cdot\beta_\mathrm{L}}\left(A_\mathrm{HDS}\,\mathrm{e}^{-E_\mathrm{HDS}/RT}C_\mathrm{L}^{1+n_\mathrm{HDS}}\right)\frac{x_{i-1}^{n_\mathrm{HDS}}x_{\mathrm{H_2}}}{1+K_{\mathrm{H_2S,HDS}}C_\mathrm{L}x_{\mathrm{H_2S}}} \tag{5}$$

- Liquid phase mass balance for the component representing the products of saturation reactions ($i = 4$):

$$\frac{\mathrm{d}(u_\mathrm{L}C_\mathrm{L}x_i)}{\mathrm{d}\ell} = \frac{\mathrm{d}}{\mathrm{d}\ell}\left(D_\mathrm{AX}C_\mathrm{L}\frac{\mathrm{d}x_i}{\mathrm{d}\ell}\right) + \frac{K_{\mathrm{LG},i}\alpha_\mathrm{V}}{\varepsilon\cdot H_\mathrm{L}}\left(\frac{C_\mathrm{G}y_i}{H_i} - C_\mathrm{L}x_i\right) + \frac{\rho_\mathrm{BED}}{\varepsilon\cdot\beta_\mathrm{L}}\left(A_\mathrm{HYD}\,\mathrm{e}^{-E_\mathrm{HYD}/RT}C_\mathrm{L}^{1+n_\mathrm{HYD}}\right)\frac{x_{i-3}^{n_\mathrm{HYD}}x_{\mathrm{H_2}}}{1+K_{\mathrm{H_2S,HYD}}C_\mathrm{L}x_{\mathrm{H_2S}}} \tag{6}$$

- Liquid phase mass balance for the dissolved hydrogen ($i = 5$):

$$\frac{\mathrm{d}(u_\mathrm{L}C_\mathrm{L}x_i)}{\mathrm{d}\ell} = \frac{\mathrm{d}}{\mathrm{d}\ell}\left(D_\mathrm{AX}C_\mathrm{L}\frac{\mathrm{d}x_i}{\mathrm{d}\ell}\right) + \frac{K_{\mathrm{LG},i}\alpha_\mathrm{V}}{\varepsilon\cdot H_\mathrm{L}}\left(\frac{C_\mathrm{G}y_i}{H_i} - C_\mathrm{L}x_i\right) - \frac{\rho_\mathrm{BED}x_{\mathrm{H_2}}}{\varepsilon\cdot\beta_\mathrm{L}}\left(\frac{S_\mathrm{HDS}\,\mathrm{e}^{-E_\mathrm{HDS}/RT}C_\mathrm{L}^{1+n_\mathrm{HDS}}A_\mathrm{HDS}x_{i-3}^{n_\mathrm{HDS}}}{1+K_{\mathrm{H_2S,HDS}}C_\mathrm{L}x_{\mathrm{H_2S}}} + \frac{S_\mathrm{HYD}\,\mathrm{e}^{-E_\mathrm{HYD}/RT}C_\mathrm{L}^{1+n_\mathrm{HYD}}A_\mathrm{HYD}x_{i-4}^{n_\mathrm{HYD}}}{1+K_{\mathrm{H_2S,HYD}}C_\mathrm{L}x_{\mathrm{H_2S}}}\right) \tag{7}$$

- Liquid phase mass balance for the hydrogen sulfide ($i = 6$):

$$\frac{\mathrm{d}(u_\mathrm{L}C_\mathrm{L}x_i)}{\mathrm{d}\ell} = \frac{\mathrm{d}}{\mathrm{d}\ell}\left(D_\mathrm{AX}C_\mathrm{L}\frac{\mathrm{d}x_i}{\mathrm{d}\ell}\right) + \frac{K_{\mathrm{LG},i}\alpha_\mathrm{V}}{\varepsilon\cdot\beta_\mathrm{L}}\left(\frac{C_\mathrm{G}y_i}{H_i} - C_\mathrm{L}x_i\right) + \frac{\rho_\mathrm{BED}\,\mathrm{e}^{-E_\mathrm{HDS}/RT}C_\mathrm{L}^{1+n_\mathrm{HDS}}}{\varepsilon\cdot\beta_\mathrm{L}}\frac{x_{\mathrm{H_2}}A_\mathrm{HDS}x_{i-4}^{n_\mathrm{HDS}}}{1+K_{\mathrm{H_2S,HDS}}C_\mathrm{L}x_{\mathrm{H_2S}}} \tag{8}$$

- Liquid phase boundary condition for all the compounds at the reactor inlet:

$$D_\mathrm{AX}C_\mathrm{L}\left.\frac{\mathrm{d}x_i}{\mathrm{d}\ell}\right|_{\ell=0} = [u_\mathrm{L}C_\mathrm{L}x_i]_{\ell=0} - [u_\mathrm{L}C_\mathrm{L}x_i]_{\ell=0^-} \tag{9}$$

- Liquid phase boundary condition for all the compounds at the reactor outlet:

$$\left.\frac{\mathrm{d}x_i}{\mathrm{d}\ell}\right|_{\ell=\mathrm{L}} = 0 \tag{10}$$

- Gas phase mass balances for all the compounds ($1 \le i \le 6$):

$$\frac{\mathrm{d}(u_\mathrm{G}C_\mathrm{G}y_i)}{\mathrm{d}\ell} = -\frac{K_{\mathrm{LG},i}\alpha_\mathrm{V}}{\varepsilon(1-\beta_\mathrm{L})}\left(\frac{C_\mathrm{G}y_i}{H_i} - C_\mathrm{L}x_i\right) \tag{11}$$

- Gas phase boundary condition for all the compounds ($1 \le i \le 6$) at reactor inlet:

$$y_i|_{\ell=0} = y_i|_{\ell=0^-} \tag{12}$$

The total continuity equations of the gas and liquid phase were combined with the above component mass balances to calculate the axial profile of the gas and liquid mean linear velocities.

- The total continuity equation for the liquid phase is

$$\frac{\mathrm{d}(u_\mathrm{L}C_\mathrm{L})}{\mathrm{d}\ell} = \frac{1}{\varepsilon\cdot\beta_\mathrm{L}}\sum_{i=1}^{6}K_{\mathrm{LG},i}\alpha_\mathrm{V}\left(\frac{C_\mathrm{G}y_i}{H_i} - C_\mathrm{L}x_i\right) - \frac{\rho_\mathrm{B}x_{\mathrm{H_2}}}{\varepsilon\cdot\beta_\mathrm{L}}\left(\frac{(S_\mathrm{HDS}-1)\,\mathrm{e}^{-E_\mathrm{HDS}/RT}C_\mathrm{L}^{1+n_\mathrm{HDS}}}{(1+K_{\mathrm{H_2S,HDS}}C_\mathrm{L}x_{\mathrm{H_2S}})}A_\mathrm{HDS}x_2^{n_\mathrm{HDS}} + \frac{S_\mathrm{HYD}\,\mathrm{e}^{-E_\mathrm{HYD}/RT}C_\mathrm{L}^{1+n_\mathrm{HYD}}}{(1+K_{\mathrm{H_2S,HYD}}C_\mathrm{L}x_{\mathrm{H_2S}})}A_\mathrm{HYD}x_1^{n_\mathrm{HYD}}\right) \tag{13}$$

and its boundary condition at the reactor inlet:

$$[u_\mathrm{L}C_\mathrm{L}]_{\ell=0} = [u_\mathrm{L}C_\mathrm{L}]_{\ell=0^-} \tag{14}$$

- The total continuity equation of the gas phase is given by the following expression:

$$\frac{\mathrm{d}(u_\mathrm{G}C_\mathrm{G})}{\mathrm{d}\ell} = -\frac{1}{\varepsilon(1-\beta_\mathrm{L})}\sum_{i=1}^{6}K_{\mathrm{LG},i}\alpha_\mathrm{V}\left(\frac{C_\mathrm{G}y_i}{H_i} - C_\mathrm{L}x_i\right) \tag{15}$$

while the boundary condition at the reactor inlet is

$$[u_\mathrm{G}C_\mathrm{G}]_{\ell=0} = [u_\mathrm{G}C_\mathrm{G}]_{\ell=0^-} \tag{16}$$

The film theory was employed to correlate the mass transfer coefficients with the effective diffusivities of the mixture compounds while the controlling mass transfer resistance at the

gas–liquid interface was presumed on the liquid side. A common film thickness (δ_L) for all the compounds was considered:

$$k_{L,i}\alpha_V = \frac{D^L_{i,\text{eff}}}{\delta_L}\alpha_V \tag{17}$$

The effective diffusivity of each mixture component in the liquid phase ($D^L_{i,\text{eff}}$) has been determined through calculations using the molecular diffusion (D^0_{ij}) and the diffusivity (D_{ij}) of the components. For the calculation of the molecular diffusion (D^0_{ij}) of a molecule i at infinite dilution in a molecule j in the liquid phase the Tyn and Calus correlation was used [12]. The respective diffusion of the dissolved gases (H_2 and H_2S) in liquid phase was estimated by Wong and Hayduk correlation [13] based on 421 data in a temperature range from 273 to 567 K. This correlation has been developed by testing several systems with numerous organic solvents and with 17 different dissolved gases except H_2. It should be mentioned that in the open literature it was not possible to find a more reliable correlation to predict the diffusion of dissolved H_2 in a petroleum fraction at hydrotreatment conditions. Besides, the correlation of Wong and Hayduk [13] gives reasonable results when compared with the Wilke and Chang correlation [14] even if the latter is not designed to estimate dissolved gas diffusion coefficients. Thereafter, the diffusivity of i and j molecules (D_{ij}) in the multicomponent mixture was calculated with Kooijman and Taylor equation [15] and finally the effective diffusivity ($D^L_{i,\text{eff}}$) of a molecule i in the mixture was estimated with Eq. (19):

$$D_{ij} = (D^0_{ij})^{x_j}(D^0_{ji})^{x_i}\prod_{k=1_{k\neq i,j}}^{n}(D^0_{ik}D^0_{jk})^{x_k/2} \tag{18}$$

$$D^L_{i,\text{eff}} = \frac{(1-x_i)}{\sum_{j=1_{j\neq i}}^{n}(x_j/D^L_{ij})} \tag{19}$$

For the calculation of D^0_{ij} with Tyn and Calus equation, the liquid viscosity and surface tension are required. The Brulé and Starling method [16] was applied to calculate liquid viscosity by neglecting the dissolved amounts of H_2 and H_2S in the organic liquid phase. For the calculations of surface tension the corresponding states correlation was applied [12]. For the application of Eq. (19) in liquid phase the true molar fractions for each compound were used.

The mathematical model of the simulation equations was numerically solved with the method of finite volumes [17]. In order to facilitate the solution of this non linear problem and to eliminate the number of repetitions of the algorithm cyclic procedure, the solution of the model by neglecting the axial dispersion and gas–liquid mass transfer terms was performed for the initialization. For the estimation of the kinetic parameters an optimization program was developed based on the method of Neadler-Mead [18].

4. Results

4.1. Apparent activity results for both reactors

In the following paragraphs the comparison of the performance of different catalytic beds as well as the effects of mass transfer and liquid non-ideal flow on reactor performance are presented and discussed employing the term ‘‘apparent activity’’. The apparent activity represents the ratio of the catalytic mass of a real reactor bed to the mass of a reference and ideal reactor achieving the same conversion at the same operating conditions. But, the apparent activity also represents the ratio of the specific reaction constant (k_{HDS}) estimated from experimental data of any catalytic bed to the specific reaction constant of a reference reactor:

$$\eta = \frac{k_{HDS}}{k_{HDS,\text{reference bed}}} \tag{20}$$

For the calculation of the apparent activity, the kinetic parameters of the HDS process were determined by using the experimental data obtained from the operation of the downflow mini-reactor diluted bed [11]. The operation of this bed is considered as a reference because it gives the highest HDS performance among the other beds tested in the frame of this work and also because there was no difference in conversion for either upflow or downflow operation (Fig. 2a). For the optimization and the parameters estimation, it was reasonably considered that this bed can be simulated as an ideal reactor and consequently the mass transfer and axial dispersion terms have been neglected. This is also supported by literature data of axial dispersion [19,20] indicating Pe higher than 85 while for the mass transfer effects it has been demonstrated that diluted small scale trickle flow reactors performance corresponds to industrial scale operation [5] which is considered free from inter-particle mass transfer effects [7]. In Fig. 2a a comparison of all the beds of both reactors in terms of sulfur concentration in the product is shown while H_2 consumption comparative results are presented in Fig. 2b.

In Fig. 2, a comparison of the operation of the bench-scale and mini-scale reactor beds is presented in terms of the apparent activity (η). Each bar of this figure corresponds to the mean apparent activity of all the experimental points of a certain bed and flow mode. On the same bar the standard deviation of catalytic activity is also shown.

As concerns the mini-reactor, it is obvious that the non-diluted bed is characterized by a reduced performance as compared with the diluted one. The performance of the diluted bed of the mini-reactor is identical in upflow and downflow mode and the apparent catalyst activity appears improved relative to the non-diluted bed. This fact consists a strong indication that the mass transfer and fluid dynamics resistances have been minimized and that this type of mini-reactor can be used as a reference reactor.

In both cases the dilution of the catalyst bed improves the apparent catalytic activity. Although the superficial velocities of each phase are the same for the corresponding experiments

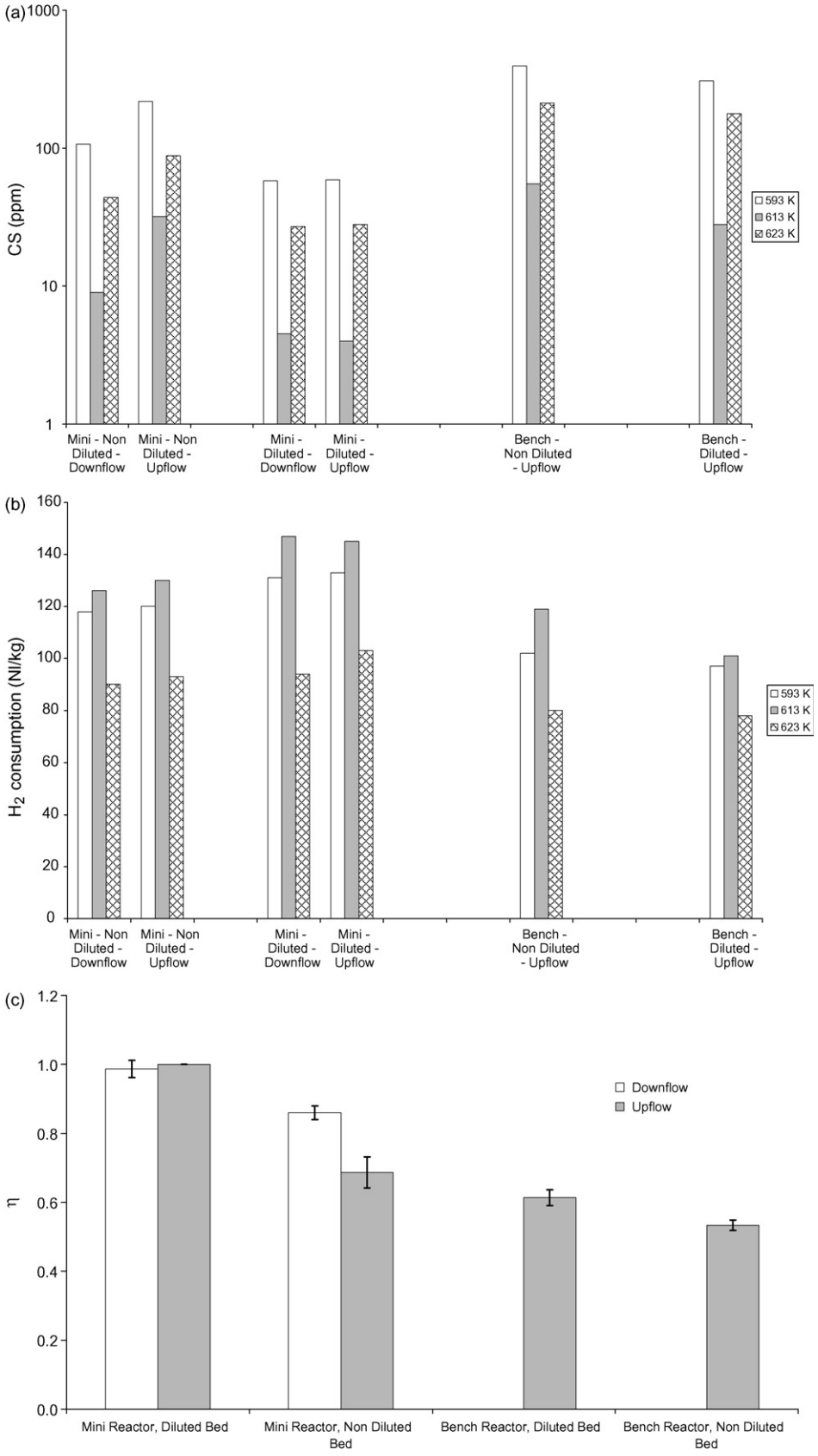

Fig. 2. (a) Comparative results of all the beds in upflow and downflow mode in terms of sulfur content in reactor effluent. (b) Comparative results of all the beds in upflow and downflow mode in terms of H_2 consumption. (c) Apparent catalytic activity for the HDS experiments of the mini- and bench-scale reactors.

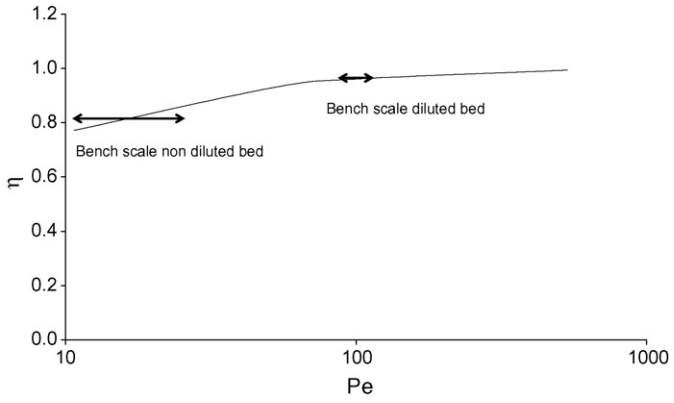

Fig. 3. Axial dispersion effects on the apparent HDS catalytic activity at T_B and P = 51 bar, WHSV = 1 h^{-1} and G/L = 1000 Nl/kg.

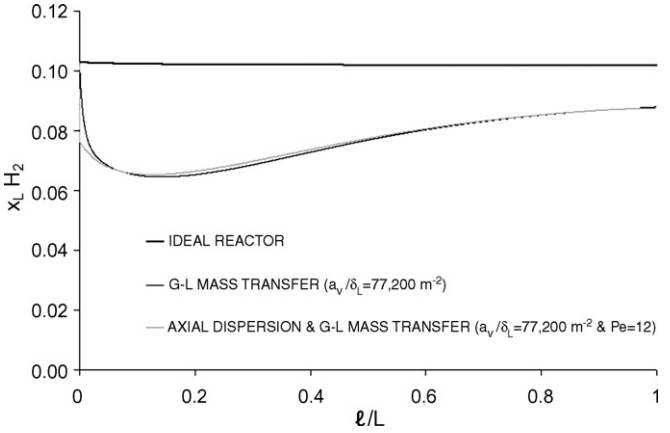

Fig. 5. Axial molar fraction profile for the diluted H_2 along the catalytic bed at T_B and P = 51 bar, WHSV = 1 h^{-1} and G/L = 1000 Nl/kg.

performed in the bench and the mini-reactors, the former reactor is not as efficient as the mini one. The biggest difference in performance is observed between the operations of the mini-scale diluted bed and the bench-scale diluted reactor and the observed important deviations are investigated in the followings.

4.2. Effect of Peclet and $K_{LG}\alpha_V$ on reactor performance

Axial dispersion and mass transfer limitations may mask reaction kinetics if not properly taken into account. In Fig. 3, a sensitivity analysis shows the dependence of the apparent catalytic activity on Peclet calculated for typical HDS conditions in an isothermal reactor, i.e. pressure of 54 bar, WHSV = 1 h^{-1} and a gas to oil ratio equal to 1000 Nl/kg. These conditions correspond to the first experimental point of Table 2. The evaluated kinetic parameters from the diluted bed of the mini-reactor are applied in this simulation and by varying the Peclet number the sulfur concentration in the reactor effluent is calculated. In a second step, axial dispersion is not taken into account but its effect is included in the estimated specific reaction constant (k_{HDS}) to achieve the same exit sulfur concentration as before but assuming ideal reactor behavior in simulation. The ratio of this reaction constant to the value of the reaction rate constant estimated from the diluted mini-scale reactor data represents the apparent activity depicted in Fig. 3. It is obvious from this figure that for Peclet numbers greater than 50 the extent of the axial dispersion effect on the apparent catalytic activity is less than 5%. The respective impact of the low gas–liquid mass transfer rates on the reaction kinetics appears stronger enough, as results from the $K_{LG}\alpha_V$ sensitivity analysis presented in Fig. 4. It is observed that apparent activity may reach values close to 0.1 while in the case of axial dispersion the value of the apparent activity is expected to be more than 0.7 for conventional operating conditions.

The main reason of the extended effect of the low mass transfer rates on reaction kinetics is that the liquid phase that irrigates the catalyst particles becomes poorer in reagents like H_2 while the product H_2S can not be easily desorbed to the gas phase. In Fig. 5, the calculated axial profile of the dissolved H_2 is presented for three different cases. It is obvious that at ideal conditions corresponding to negligible mass transfer resistances and dispersion the diluted hydrogen in the liquid phase is almost constant as it is fed in excess. On the contrary, in a reactor where the mass transfer resistances are strong enough (α_V/δ_L = 77,200 m^{-2}), a lack of hydrogen in the liquid phase is

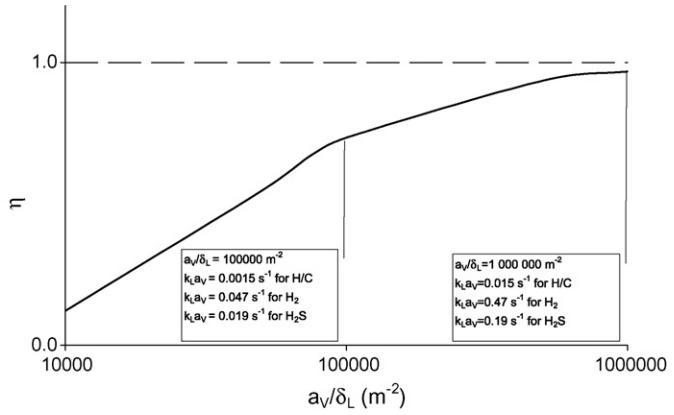

Fig. 4. Gas–liquid mass transfer masking effect on the apparent HDS catalytic activity at T_B and P = 51 bar, WHSV = 1 h^{-1} and G/L = 1000 Nl/kg.

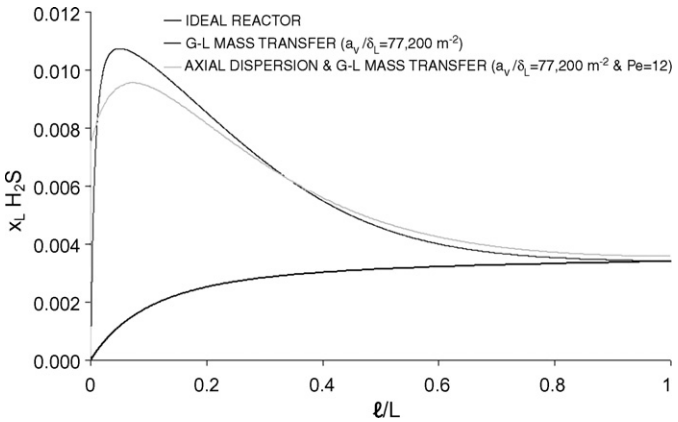

Fig. 6. Axial molar fraction profile for the diluted H_2S along the catalytic bed at T_B and P = 51 bar, WHSV = 1 h^{-1} and G/L = 1000 Nl/kg.

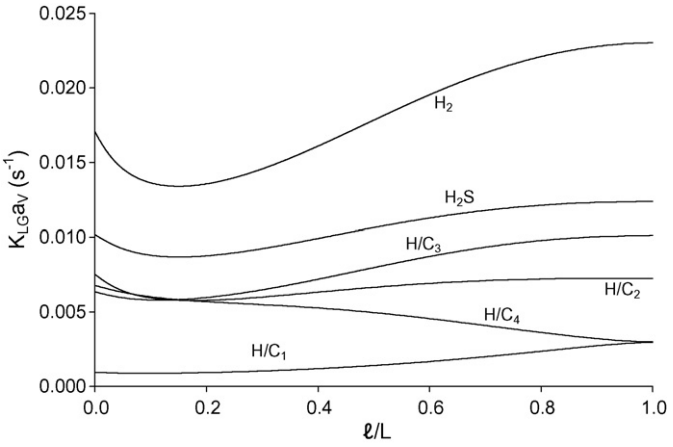

Fig. 7. Variation of $K_{LG}\alpha_V$ values along the catalyst bed corresponding to $\alpha_V/\delta_L = 77{,}200\ m^{-2}$ at T_B and $P = 51$ bar, WHSV = 1 h^{-1} and $G/L = 1000$ Nl/kg.

observed close to the reactor inlet because of its high consumption rates and its insufficient renewal via the gas–liquid interface. If beside the mass transfer resistances the axial dispersion is considered not negligible ($Pe = 12$) then the curve of hydrogen profile is a little more spread due to the dispersion in the liquid phase along the axis, but very close to the curve drawn for mass transfer resistances only. In Fig. 6, the axial profile of the diluted hydrogen sulfide is plotted for the corresponding conditions of Fig. 5. For the ideal reactor operation it appears that H_2S concentration increases along the reactor length due to the reaction progress. In the case of existence of mass transfer resistance ($\alpha_V/\delta_L = 77{,}200\ m^{-2}$) an accumulation of H_2S in the liquid phase is observed close to the reactor entrance where its production rates are high and its desorption into the gas phase is restricted by low mass transfer rates. The same conclusion arise from the profile calculated when both axial dispersion ($Pe = 12$) and mass transfer ($\alpha_V/\delta_L = 77{,}200\ m^{-2}$) are taken into account. The only difference is that in the latter case, the curve is more spread as also the respective profile of diluted hydrogen in Fig. 5. The gas–liquid mass transfer coefficients at the inlet of the catalytic bed that correspond to $\alpha_V/\delta_L = 77{,}200\ m^{-2}$ are: $K_{LG,H/C}\alpha_V = k_{L,H/C}\alpha_V = 0.00075\ s^{-1}$; $K_{LG,H_2}\alpha_V = k_{L,H_2}\alpha_V = 0.0235\ s^{-1}$; $K_{LG,H_2S}\alpha_V = k_{L,H_2S}\alpha_V = 0.0095\ s^{-1}$. These values change along the length of the bed as they depend on the composition of the mixture. The change of these values is portrayed in Fig. 7 and it is observed that their deviations cannot be neglected in solving the simulation model.

4.3. Estimation of mass transfer effects

For the estimation of the extent of the mass transfer resistances on the operation of the bench-scale and mini-scale beds the corresponding gas–liquid mass transfer coefficients must be available. To the best of our knowledge there is no available gas–liquid mass transfer data for such small fixed bed gas–liquid reactors at hydrotreatment conditions. An excellent review has been published by Larachi et al. [21] who have developed a neural network for the estimation of $k_L\alpha_V$, $k_G\alpha_V$ and α_V by using 902, 498 and 1484 data, respectively, issued from trickle bed systems. In the same work the authors mention that for the upflow mode they treated 439 and 499 data for $k_L\alpha_V$ and α_V, respectively, but they did not find data for $k_G\alpha_V$ in the open literature. Besides, their data for upflow operation was not enough to develop a reliable neural network for $k_L\alpha_V$.

For the estimation of the gas–liquid mass transfer coefficient in this work, it was considered that the reference catalytic activity is the one corresponding to experiments performed with the diluted mini-reactor. The axial dispersion coefficients and the liquid hold up for the catalyst beds operating in the upflow mode have been evaluated from mock up experiments [19,20]. Their values are correlated with the liquid and gas superficial velocities as shown in the following Eqs. (21) and (22). The constants of these empirical correlations are given in Table 3:

$$\beta_L = c_1 u_{GS}^{c_2} \tag{21}$$

$$D_{AX} = c_3 \frac{u_{LS}^{c_4} u_{GS}^{c_5}}{1 + c_6 u_{GS}} \tag{22}$$

In Table 4, the calculated values of liquid hold up, axial dispersion coefficient and Peclet number are given for the non-diluted and diluted bed of the bench reactor operating in upflow mode. The axial dispersion is more extended in the non-diluted bed as compared with the diluted one and the Peclet number of the diluted bed is from 4 to 10 times higher than those of the non-diluted. In the diluted bed Peclet number is greater than 90. Referring to Fig. 3, it is concluded that the impact of the back mixing on the apparent catalytic activity is less than 4% and so the performance deviations observed between the diluted bed of the bench-scale and of the mini-reactor is mostly attributed to mass transfer restrictions of the former.

By using the optimization code, the optimum mass transfer coefficient value for each experimental point was calculated in such a way as to converge each predicted product sulfur concentration to the real value. By considering that the film length is common for all the compounds it was possible to

Table 3
The constants values for the correlation of hold up and axial dispersion

	c_1	c_2	c_3	c_4	c_5	c_6
Non-diluted	0.734	−0.035	3.1	0.042	0.072	0.53
Diluted	0.704	0.0353	7.6	0.756	0.823	1.11

Table 4
Simulated axial dispersion and liquid hold up values for the non-diluted and the diluted bed of the bench-scale upflow reactor

WHSV (h^{-1})	T (K)	Bed					
		Non-diluted			Diluted		
		β_L	D_{AX} ($mm^2\ s^{-1}$)	Pe	β_L	D_{AX} ($mm^2\ s^{-1}$)	Pe
1.0	593	0.723	1.54	12	0.715	0.33	97
1.0	613	0.722	1.48	9	0.716	0.25	87
2.0	623	0.722	1.55	27	0.805	0.59	115

Table 5
Estimated liquid-side mass transfer coefficient for the beds of the bench and mini-scale reactors

T (K)	Bench-scale reactor						Mini-scale reactor		
	Non-diluted bed			Diluted bed			Non-diluted bed		
	α_V/δ_L (m^{-2})	$k_{L,H/C}\alpha_v$ (s^{-1})	$k_{L,H_2}\alpha_v$ (s^{-1})	α_V/δ_L (m^{-2})	$k_{L,H/C}\alpha_V$ (s^{-1})	$k_{L,H_2}\alpha_V$ (s^{-1})	α_V/δ_L (m^{-2})	$k_{L,H/C}\alpha_V$ (s^{-1})	$k_{L,H_2}\alpha_V$ (s^{-1})
593	77200	0.0012	0.036	51800	0.0008	0.024	235,000	0.0035	0.110
613	68400	0.0012	0.036	52300	0.0009	0.028	149,000	0.0027	0.078
623	74300	0.0015	0.041	58700	0.0012	0.033	190,000	0.0034	0.100

calculate first the optimum α_V/δ_L value and thereafter the $k_{Li}\alpha_V$ value for every compound.

In Table 5, the mass transfer results are presented having attributed all the mass transfer resistances to the liquid phase film at the gas–liquid interface. First, it appears that the α_V/δ_L values in the case of the non-diluted bed of the bench reactor are systematically higher than those of the bench-scale diluted bed despite the improved HDS performance of the latter (Fig. 2). This indicates that dilution has a negative effect on mass transfer in the case of the bench-scale reactor. But, dilution of mini-scale catalyst beds decreases the mass transfer effects. This opposite trend of gas–liquid mass transfer resistances with catalyst bed dilution in the different reactor scales shows that the flow regime is not the same in the reactors of different scale. Moreover, the α_V/δ_L values corresponding to both beds of the bench reactor are much lower than the α_V/δ_L values of the mini-scale non-diluted bed. This fact justifies the performance difference between the two reactors.

4.4. Interpretation of the results

The different extent of the two phase mass transfer phenomena that take place in these reactors is attributed to the much lower (10 times less) cross section area of the mini-reactor. As the operating conditions for the corresponding experiments in mini- and bench-scale reactor beds were exactly the same the bubble size is expected to be the same. Optical observation of mock-up experiments with analogous beds and conditions to those prevailing in hydrotreatment have indicated that the position at which the gas bubbles came out at the top of the bench-scale beds, either diluted or non-diluted, scarcely changed with time and the bubbles were well apart from each other (Fig. 8). This indicates that the bubbles follow certain paths through the bed well apart from each other leading to poor gas–liquid contact. Building a mini-reactor with a smaller diameter the gas–liquid distribution is improved even if only one way for the bubbles passage is created through the mini-scale bed. Therefore, the concentration of the hydrogen and hydrogen sulfide along the reactor radius is more uniform and closer to the thermodynamic saturation. Poor gas bubbles distribution in bench-scale beds results in some almost saturated with H_2 areas close to the interface along the preferential paths that bubbles follow through the bed but there are areas where H_2 has been consumed and the transfer rates are not sufficient to renew it. In parallel, in the hydrogen depleted areas a concentration maximum of H_2S produced during HDS is developed inhibiting the catalytic reactions. In Fig. 8, a schematic representation of the bubble distribution at the top of the bench and mini-scale bed is presented along with the concentration profiles of the dissolved gases in the liquid phase for both reactors. It is shown that the profiles in the mini-reactor are expected to be more uniform as the transfer distances in the liquid phase along the bed radius are shorter.

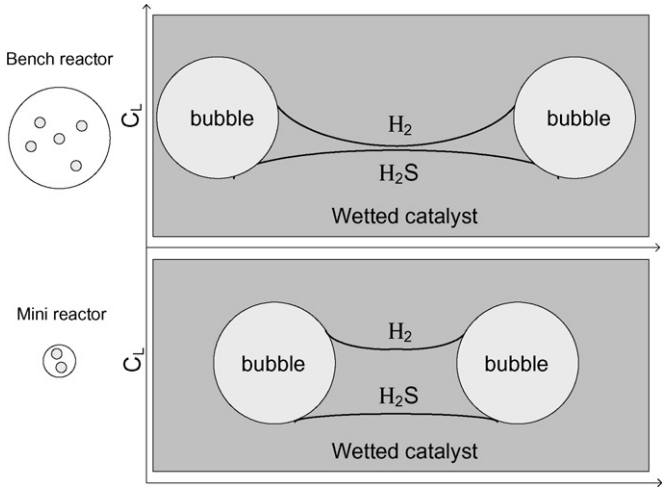

Fig. 8. Graphic depiction of the bubbles distribution at the top of the catalyst beds and of the radial distribution of dissolved gases in the liquid phase between two passages of gas bubbles.

The higher mass transfer coefficients for the non-diluted bench-scale bed as compared with the diluted one can be attributed to the decreased mass transfer rates to and from the paths of the gas bubbles due to the reduced mixing around the bubbles imposed by the smaller void fraction of the diluted structure. For the mini-scale reactor, however, with improved gas–liquid contact as described above, mass transfer rates in the diluted bed are higher than in the non-diluted one.

5. Conclusions

The mass transfer effects on the gas oil hydrodesulphurization performance of two laboratory reactors with different geometry have been investigated. It has been shown that mass transfer resistances which also reflect the effective gas–liquid contact appear to be significant. The bed dilution with inert fines improves the apparent catalytic activity but the reactor geometry and size strongly affect the reactor performance. For the cases and the conditions studied the mini-reactor is

characterized by a better performance resulting from a more efficient gas–liquid contact and higher mass transfer rates than those prevailing in the bench-scale reactor.

References

[1] J.V. Klinken, R.H.V. Dongen, Catalyst dilution for improved performance of laboratory trickle-flow reactors, Chem. Eng. Sci. 35 (1980) 59–65.

[2] Y. Wu, M.R. Khadilkar, M.H. Al-Dahhan, M.P. Dudukovic, Comparison of upflow and downflow two-phase flow packed-bed reactors with and without fines: experimental observations, Ind. Eng. Chem. Res. 35 (1996) 397–405.

[3] M.H. Al-Dahhan, M.P. Dudukovic, Catalyst bed dilution for improving catalyst wetting in laboratory trickle-bed reactors, AIChE J. 42 (1996) 2594–2606.

[4] M.H. Al-Dahhan, F. Larachi, M.P. Dudukovic, A. Laurent, High-pressure trickle-bed reactors: a review, Ind. Eng. Chem. Res. 36 (1997) 3292–3314.

[5] S.T. Sie, Miniaturization of hydroprocessing catalyst testing systems: theory and practice, AIChE J. 42 (1996) 3498–3507.

[6] H. Gierman, Design of laboratory hydrotreating reactors scaling down of trickle-flow reactors, Appl. Catal. 43 (1988) 277–286.

[7] S.T. Sie, R. Krishna, Process development and scale up. III. Scale up and scale down of trickle bed processes, Rev. Chem. Eng. 14 (1998) 203–252.

[8] D. Letourneur, R. Bacaud, M. Vrinat, D. Schweich, I. Pitault, Hydrodesulfurization catalyst evaluation in an upflow three-phase microreactor, Ind. End. Chem. Res. 37 (1998) 2662–2667.

[9] S.K. Ajmera, C. Delattre, M.A. Schmidt, K.F. Jensen, Microfabricated differential reactor for heterogeneous gas phase catalyst testing, J. Catal. 209 (2002) 401–412.

[10] K.F. Jensen, Microreaction engineering—is small better, Chem. Eng. Sci. 56 (2001) 293–303.

[11] G.D. Bellos, N.G. Papayannakos, The use of a microreactor to investigate HDS kinetics, Catal. Today 79/80 (2003) 349–355.

[12] R.C. Reid, J.M. Prausnitz, B.E. Poling, The Properties of Gases and Liquids, 4th ed., McGraw-Hill, Singapore, 1988.

[13] C.F. Wong, W. Hayduk, Correlations for prediction of molecular diffusivities in liquids at infinite dilution, Can. J. Chem. Eng. 68 (1990) 849–859.

[14] C.R. Wilke, P. Chang, Correlation of diffusion coefficients in dilute solutions, AIChE J. 1 (1955) 264–270.

[15] H.A. Kooijman, R. Taylor, Estimation of diffusion coefficients in multicomponent liquid systems, Ind. Eng. Chem. Res. 30 (1991) 1217–1222.

[16] M.R. Brulé, K.E. Starling, Thermophysical properties of complex systems: applications of multiproperty analysis, Ind. Eng. Chem. Process Des. Dev. 23 (1984) 833.

[17] H.K. Versteeg, W. Malalasekera, Computational Fluid Dynamics, 1st ed., Longman Scientific & Technical, Essex, 1995.

[18] G.R. Walsh, Methods of Optimization, Wiley, New York, 1979.

[19] A.M. Thanos, Non Ideal Flow of Upflow Pilot Hydrotreaters, PhD Dissertation, National Technical University of Athens, Greece, 1997.

[20] A.M. Thanos, G.D. Bellos, P.A. Galtier, N.G. Papayannakos, Bed length effect on the liquid phase non-idealities and holdup in pilot scale upflow reactors, Catal. Today 79–80 (2003) 235–240.

[21] F. Larachi, L. Belfares, I. Iliuta, B.P.A. Grandjean, Heat and mass transfer in cocurrent gas–liquid packed beds. Analysis, recommendations and new correlations, Ind. Eng. Chem. Res. 42 (2003) 222–242.